DOI 10.1515/aot-2013-0045 — Adv. Opt. Techn. 2014; 3(2): 199–207

**Research Article**

Dirk Roessler[a,]*, David A.K. Pedersen, Mathias Benn and John L. Jørgensen

# Optical stimulator for vision-based sensors

**Abstract:** We have developed an optical stimulator system for vision-based sensors. The stimulator is an efficient tool for stimulating a camera during on-ground testing with scenes representative of spacecraft flights. Such scenes include starry sky, planetary objects, and other spacecraft. The optical stimulator is used as a test bench to simulate high-precision navigation by different types of camera systems that are used onboard spacecraft, planetary rovers, and for spacecraft rendezvous and proximity maneuvers. Careful hardware design and preoperational calibration of the stimulator result in high precision and long-term stability. The system can be continuously used over several days. By facilitating a full camera including optics in the loop, the stimulator enables the more realistic simulation of flight maneuvers based on navigation cameras than pure computer simulations or camera stimulations without the involvement of the actual optics.

**Keywords:** flight simulator; optical stimulator; rendezvous and proximity maneuver; spacecraft attitude; star tracker camera; vision-based navigation.

[a]Now at: GFZ German Research Centre for Geosciences, Potsdam, Germany

***Corresponding author: Dirk Roessler,** National Space Institute, Division Measurements and Instrumentation, Technical University of Denmark, Elektrovej 327, room 221, 2800 Kgs. Lyngby, Denmark, e-mail: d-roessler@web.de

**David A.K. Pedersen, Mathias Benn and John L. Jørgensen:** National Space Institute, Division Measurements and Instrumentation, Technical University of Denmark, Elektrovej 327, room 221, 2800 Kgs. Lyngby, Denmark

## 1 Introduction

Since the pioneering development of star tracker cameras such as the Advanced Stellar Compass [1], the microAdvanced Stellar Compass [2], and others [3], digital cameras have been successfully used for autonomous attitude determination of spacecraft based on the observation of stars. Accurate relative range and attitude determination as well as fully autonomous rendezvous and proximity operations between spacecraft by means of vision-based navigation have proven feasible since the development of the vision-based sensor (VBS) [4]. Such sensor systems will be of growing importance for future proximity, rendezvous, and docking maneuvers between spacecraft as well as for landing of spacecraft on planets and other celestial bodies.

Spacecraft maneuvers require careful preparation, realistic simulations, and testing. On-ground flight simulations with flight-representative test benches are cost-effective and flexible alternatives to expensive in-flight tests. Owing to the key role of camera systems for spacecraft attitude control and navigation, the involvement of the physical camera during such simulations and testing of maneuvers increases the representativeness of a test bench.

Therefore, different approaches have been followed to develop star tracker stimulators for different real cameras in the loop [5, 6]. The Optical Stimulator for Vision-Based Sensors (OSVBS) has been developed, verified, and tested by the National Space Institute of the Technical University of Denmark. It enables the flexible stimulation of a variety of navigation cameras in open and closed loop and can be embedded within complex test benches [7]. Here, we describe the mechanical and software setup of the OSVBS as well as results from testing.

## 2 System setup

The main objective of the OSVBS is the realistic stimulation of navigation cameras with flight scenarios in space. The scenarios include spacecraft navigation based on star observations as well as rendezvous and proximity operations between spacecraft or between a spacecraft and celestial bodies. Typically, scene rendering by software [8, 9] results in perfect images. However, actual camera images are distorted due to the involved optics, electronics, and software. The effects include geometric distortion

and noise. For realistic simulations of optical navigation, a camera including the optics must therefore be stimulated and included in the loop.

OSVBS supports a wide range of real navigation cameras, without the need for major modifications. The cameras are stimulated in the loop by static or dynamic monitor images that are viewed by the camera optics (Figure 1). The images represent scenes in space and are characterized by high fidelity, appropriate geometry, and intensity.

The main criteria of the system's design are

1. Ability to stimulate different camera systems with high fidelity,
2. Modularity such that the main individual components can be replaced,
3. Cost efficiency by using components off the shelf.

## 2.1 Hardware

The modular hardware design of OSVBS mainly consists of a standard desktop PC as scene calculator and an optical stimulator. The optical stimulator is connected to the PC and hosts the camera optics.

The scene calculator generates the scene images. Taking into account the sensor's dimensions and the focal length of the mounted camera, space-representative color images are computed utilizing PANGU [8], but other simulator software such as Celestia [9] can also be used. In this way, the generic images appear as perfect space images without involving the optics and the electronics of the camera. Scene control is realized based on commands from an external real-world simulator (Figure 2) and an external timing system that enables near real-time commanding. The command interface is defined by the involved software used for the scene generation.

The hardware of the optical stimulator in the loop includes a standard 24″ LED monitor with 1900×1200 px screen resolution. The monitor receives video input from the scene calculator, and it is this that is used for the camera stimulation.

A carefully designed optical bench connects the monitor to the camera tower, which hosts the camera being involved (Figure 1, left). The camera tower hosts the mechanical interface to the camera. Cameras with a wide range of physical dimensions can be considered. Together with the optical bench, the camera tower provides stable and adjustable connection to the stimulator monitor. The camera mount, itself, depends upon the camera. An additional camera adapter may be required between the camera and the mechanical interface (Figure 1, right). The different stages of the camera tower (Figure 1, right) allow a 3 DoF (degree of freedom) adjustment of the camera, namely, translation along the optical bench and rotation approximately about yaw and pitch of the camera. Translations between 0 and 1850 mm are supported. The yaw and pitch adjustment enables the pointing of the camera toward the monitor. Orienting the camera to within 1° to the normal of the monitor can be done rapidly with the remaining geometric distortions compensated for by the software.

An additional optic, being specific to the camera, in front of the camera lens may be required for the correct

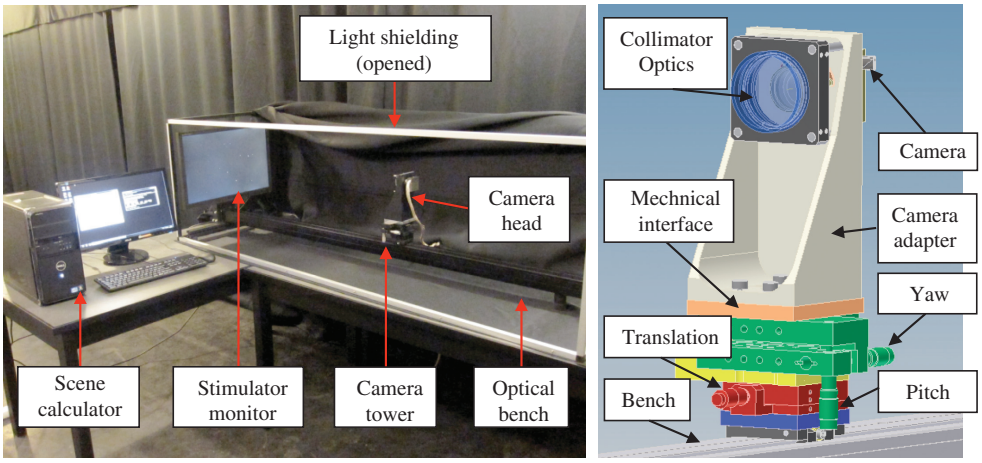


**Figure 1** System setup. Left: OSVBS with mounted camera head. The light shielding is opened to allow viewing of the inner part. Right: CAD drawing of the camera tower sitting on the bench with the camera mounted through the camera adapter to the mechanical interface atop the 3 DoF (degree of freedom) stage (2 DoF rotations, 1 DoF translation along the bench).

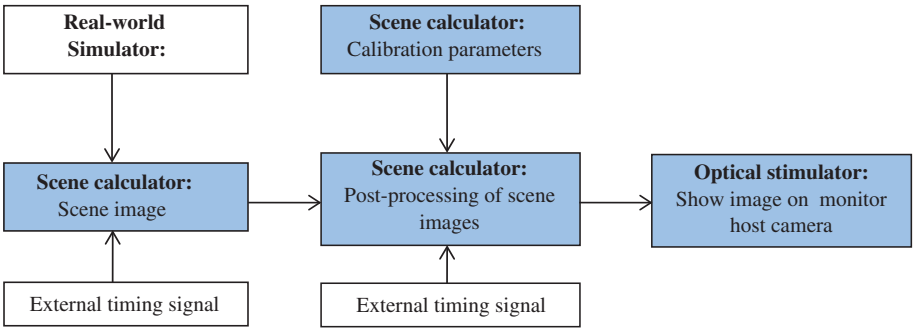


**Figure 2** Process flow of signal generation for the camera stimulation commanded by the Real-World Simulator. Blue boxes indicate components of the OSVBS.

focusing of the camera on the monitor, in combination with the translation stage. In the case of DTU's microASC [2], one standard 1000-mm collimator lens is used. The lens surface is coated to suppress reflections of light in the wavelength range of 400–700 nm, e.g., multipathing between the camera lens and the collimator. Mounted on the camera adapter, the lens is placed directly in front of the camera lens.

The optical stimulator is shielded against secondary light (Figure 1, right). The modular system setup allows for the easy replacement of individual hardware items such as the monitor and software components such as the scene generator and the use of different camera models in the loop.

## 2.2 Software

In order to make use of the high precision of the considered navigation systems (e.g., microASC [2]), it is essential that the geometry of the image projected onto the monitor is extremely accurate. While the accurate mechanical alignment of the camera with respect to the monitor is provided by the camera tower, variations in camera roll are not supported. Furthermore, the fine adjustment of the camera's pointing to better than a few tens of a degree can be extremely time consuming and is not performed. However, the resulting geometric distortions can be easily corrected by software. Likewise, the involvement of additional optics and the camera lenses result in distortion of the field-of-view of the camera, which must also be accounted for after image generation by the PC.

Therefore, software is applied to account for lens distortion and for position and pose of the optical system by image manipulation applied to the generic images. The image manipulation is carried by a combination of preoperational optical calibration and image postprocessing in the loop. Both are carried out using software developed at DTU Space on the basis of OpenCV [10] libraries.

### 2.2.1 Optical calibration

Let $(x_p, y_p, F)$ be a point on the sensor chip of a perfect pinhole camera and $(X, Y, Z)$ be the coordinates of a viewed object in the same coordinate frame [10]. Then,

$$\begin{bmatrix} x_p \\ y_p \end{bmatrix} = \begin{bmatrix} f_x X/Z + c_x \\ f_y Y/Z + c_y \end{bmatrix}, f_x = Fs_x, f_y = Fs_y,$$

where $(s_x, s_y)$ and $(c_x, c_y)$ are pixel densities and the coordinate of the principle point along the $x$- and $y$-axis of the sensor chip, and $F$ is the effective focal length of the camera. We assume that $(s_x, s_y)$ is known from the camera manufacturer or from the camera's calibration.

Owing to radial and tangential distortion of the image by the camera lens system, points $(x_p, y_p)$ are really in the wrong position $(x_d, y_d)$

$$\begin{bmatrix} x_p \\ y_p \end{bmatrix} = (1 + k_1 r^2 + k_2 r^4 + k_3 r^6) \begin{bmatrix} x_d \\ y_d \end{bmatrix} + \begin{bmatrix} 2p_1 x_d y_d + p_2 (r^2 + 2x_d^2) \\ p_1 (r^2 + 2y_d^2 + 2p_2 x_d y_d) \end{bmatrix},$$

where $k_i$ and $p_i$ are distortion coefficients describing the radial and tangential lens distortion, respectively, and $r$ is geometric distance of $(x_d, y_d)$ from the principle point in the sensor plane.

The parameters $(s_x, s_y)$, $(c_x, c_y)$, $F$, $p_i$, and $k_i$ are the intrinsic parameters. $(c_x, c_y)$, $p_i$, and $k_i$ are to be determined by calibration. They result from the combination of the camera lens and the additional optics in front of the camera. The distortion $\boldsymbol{d}$ vector is formed such that $\boldsymbol{d} = [k_1 \; k_2 \; p_1 \; p_2 \; k_3]^T$.

The extrinsic parameters describe the rotation and translation of a viewed object with respect to the camera. They are given by the homography, a projective mapping

between two planes. We define the viewed object point $\boldsymbol{Q}$ with $\tilde{\boldsymbol{Q}}=[XYZ1]^T$ and $\tilde{\boldsymbol{q}}=[x_p\ y_p\ 1]^T$. The translation $\boldsymbol{T}$ between a point in the plane of the camera sensor and a point on a viewed plane is $\boldsymbol{T}=origin_{viewed}\text{-}origin_{camera}$. The 3D rotation between the two planes is described by the rotation matrix $\boldsymbol{R}$. With $\boldsymbol{M}=\begin{bmatrix} f_x & 0 & c_x \\ 0 & f_y & c_y \\ 0 & 0 & 1 \end{bmatrix}$, $\boldsymbol{W}=[\boldsymbol{RT}]$, and $\boldsymbol{R}=[\boldsymbol{r}_1\ \boldsymbol{r}_2\ \boldsymbol{r}_3]$, the transformation between $\tilde{\boldsymbol{q}}$ and $\tilde{\boldsymbol{Q}}$ is given by

$$\tilde{\boldsymbol{q}}=s\boldsymbol{MW}\tilde{\boldsymbol{Q}},$$

where $s$ is an arbitrary scaling factor. Assuming that $\boldsymbol{Q}$ lies on a plane through the origin of the viewed plane, $Z=0$. Then

$$\tilde{\boldsymbol{q}}=\begin{bmatrix} x_p \\ y_p \\ 1 \end{bmatrix}=s\boldsymbol{M}[\boldsymbol{r}_1\boldsymbol{r}_2\boldsymbol{r}_3\boldsymbol{T}]\begin{bmatrix} X \\ Y \\ 0 \\ 1 \end{bmatrix}=s\boldsymbol{M}[\boldsymbol{r}_1\boldsymbol{r}_2\boldsymbol{T}]\begin{bmatrix} X \\ Y \\ 1 \end{bmatrix}\text{and } \tilde{\boldsymbol{q}}=s\boldsymbol{H}\widetilde{\boldsymbol{Q}'}.$$

Here, $\boldsymbol{H}$ is the 3×3 homography matrix. The inverse of the homography matrix can be used to project the given points in the plane of the camera to the other plane such as a monitor. Therefore, $\boldsymbol{H}$ contains all the sought extrinsic parameters.

The intrinsic parameters and $\boldsymbol{H}$ are sought during the calibration of the optical system representing the entire optical system including the camera and the additional optics. Application of them enables the correct projection of the image in the field-of-view of the camera as it would be in nature.

For calibration, a well-known chessboard pattern projected onto the monitor is viewed by the camera. The conditions for homography are met as both the camera sensor and the viewed monitor screen form planes. For calibration of intrinsic and extrinsic parameters, OpenCV routines [10] are applied to downloaded camera images. The corner positions of the chessboard are extracted at subpixel accuracy and associated with the corner positions of the generic image. The intrinsic parameters are first determined in an attempt to straighten all lines connecting the points in x and y directions [11, 12]. Corner positions are corrected for lens distortion based on the determined intrinsic parameters. The homography matrix is computed by comparison of the corrected corner positions on the camera sensor and the known values on the monitor. The translation vector as well as pitch, yaw, roll of the camera are derived from the homography matrix [10].

Initially, the extrinsic parameters are considered for the mechanical adjustment of the camera pointing within 1°. The final optical calibration is carried out based on several, up to 10, uncompressed camera images from a single, projected chessboard image. Calibration is required only once prior to the operation of OSVBS. Depending on the download speed of the camera, typical calibrations are time efficient and take no more than 10 min. Thereafter, the system can be used for several days without interruption, given that temperatures are stable. The extrinsic calibration parameters can also be used to assist opto-mechanical adjustment of the camera.

### 2.2.2 Image manipulation

Based on the determined intrinsic and extrinsic calibration parameters, the image manipulation SW adjusts the images at subpixel accuracy and projects them on the stimulator monitor. The matrices $\boldsymbol{M}$, $\boldsymbol{H}$, and $\boldsymbol{d}$ are employed to compute rectification look-up maps using the OpenCV routine cvInitUndistortRectifyMap() [10]. The look-up maps contain the mapping from the pixels of the monitor to the pixels of the camera. They are used in the OpenCV routine cvRemap() [10] to manipulate the generic images and project them onto the monitor. In this way, the image projection is efficient, and projected images attain an extremely accurate geometry with respect to the viewing camera.

The camera stimulation is synchronized to an external clock by a pulse-per-second (PPS) signal or to the internal clock of the scene calculator.

The optical stimulator is embedded in an on-ground test bench (Figure 3) where it can be operated in open and closed loop modes. When connected to the stimulator, the camera operates independently of the OSVBS. Only for calibration, camera-taken images must be uploaded to the computer. Depending on the camera, the direct sending and receiving of telemetry and telecommand (TM/TC) packages may be possible by the computer.

## 3 Accuracy

The accuracy of the geometry of the projected images is given by the performance of the optical calibration and image manipulation. OSVBS reaches a high level of scene accuracy, in-flight representativeness, and high long-term stability. The accuracy of the projected images is tested based on projected star images viewed by DTU's micro-ASC [2]. Like in standard operation, the microASC computes the camera attitude based on the stars in the images

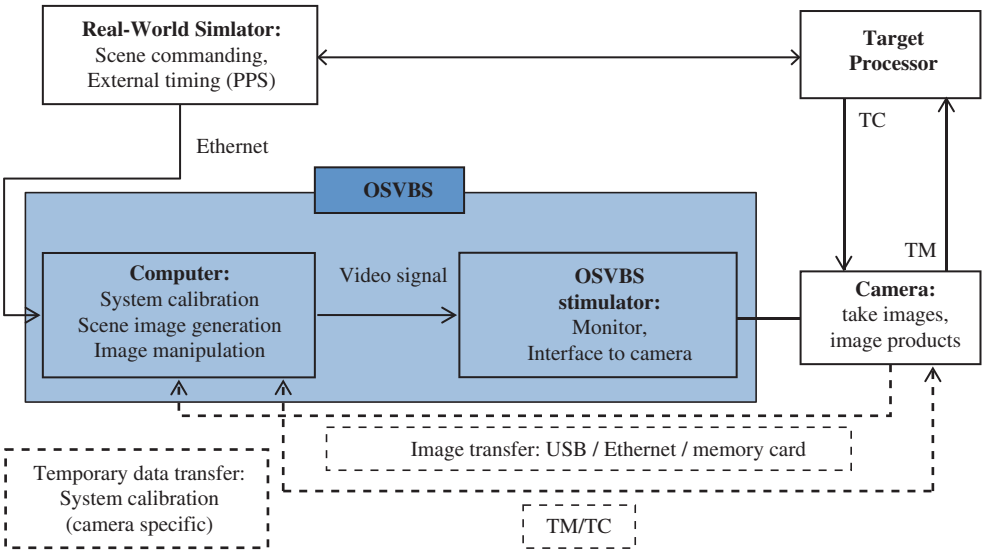


**Figure 3** OSVBS embedded in a possible on-ground test bench with the camera, Target Processor, and Real-World Simulator in closed loop. Straight lines show essential connections during close-loop operation. Dashed lines show optional connections during calibration where TM/TC package can also be transmitted using another computer.

shown on the monitor. The camera solutions are compared to values used for image generation.

Owing to system calibration and hyper-accuracy image manipulation, the accuracy of the projected images as given by the attitude solutions of DTU's microASC [2] is always better than 20 arcsec for yaw and pitch and better than 200 arcsec for roll. Typically, these values are significantly below 10 arcsec and 100 arcsec, respectively.

In thermally stable environments, the system has been continuously operated without loss of accuracy for more than 20 h and up to 1 week without re-calibration. Therefore, the stimulator can be used to simulate ambitious space flight maneuvers. The requirement to perform re-calibration can be tested by the stimulation of the camera using static star images or other calibrated images.

# 4 Test examples

OSVBS has been carefully tested and used along with DTU's microASC [2] and VBS camera [4] (Figure 4). Onboard a spacecraft, the microASC/VBS autonomously determines the attitude of the camera, itself, based on star observations. It also measures the line-of-sight angles of nonstellar objects such as spacecraft in the field-of-view of the camera. The parameters can then be related to other coordinate systems such as that of the spacecraft. The camera has a typical pointing accuracy of about 1 arcsec in right ascension and declination in the J2000.0 coordinate system.

For testing the accuracy of the image geometry and the scene fidelity, the camera is stimulated with scene images projected onto the monitor. Such scenes represent starry sky or other spacecraft. Static and dynamic scenes are considered. As onboard a spacecraft, the camera is used autonomously to determine the attitude parameters and the line-of-sight parameters. The solutions are retrieved by telemetry/telecommands sent between the camera and another external PC connected to the camera. All tests are performed using the calibration parameters obtained from standard system calibration before the tests.

## 4.1 Static starry-sky scenes

Static images representing starry sky are a simple yet powerful means to assess the image fidelity. In the case of the microASC, small image distortions will result in obscured or even invalid camera solutions. The quality of

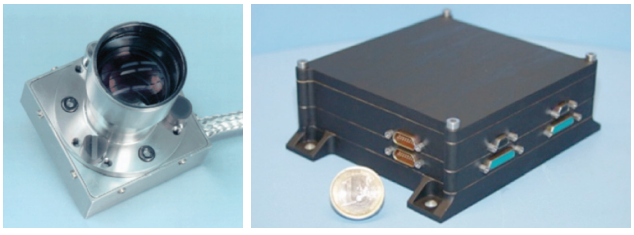

**Figure 4** Camera head unit (left) and data processing unit (right) of DTU's microASC [2] and VBS [4].

the viewed images is therefore assessed by comparison of the attitude values assumed for the image generation with the camera solution.

Involving OSVBS for camera stimulation, high-precision camera attitude solutions are obtained (Table 1, Figure 5). The obtained uncertainties in attitude angles are very low (Table 1) and close to the values for camera operations in space. Therefore, the image geometry is highly representative of real scenes.

The obtained results are representative for the operation of OSVBS with still images where the average pointing precisions are typically below 10 arcsec for right ascension and declination and always better than 20 arcsec. Standard deviations are <10 arcsec.

**Table 1** Mean and standard deviation $\sigma$ of the differences $\Delta$ between angles from camera attitude solutions and generic values (compare Figure 5).

| | Mean ($\Delta$) | $\sigma$ |
|---|---|---|
| $\Delta$(*ra*) (right ascension) | 0.2″ | 2.8″ |
| $\Delta$(*dec*) (declination) | 1.2″ | 3.4″ |
| $\Delta$(*rot*) (rotation) | 8.1″ | 54.5″ |

The viewed image is static, representing starry sky. Angles: *ra*, right ascension; *dec*, declination; *rot*, rotation in J2000.0 coordinate frame.

## 4.2 Dynamic starry-sky scenes

Dynamic star scenes represent scenes with transient changes in the attitude of the camera. Such scenarios correspond to a rotation of the camera, e.g., by the rotation of the spacecraft while orbiting Earth.

An analysis of dynamic scenes is used for the evaluation of the representativeness of the scenes together with the timing of OSVBS and the camera. A realistic flight-representative simulation has been carried out by mimicking attitudes measured by one of DTU's star-tracker camera onboard of the PRISMA satellite [4] during one orbit (Figure 6).

Attitudes assumed for image generation and attitudes obtained by the camera viewing the monitor (Figure 6) are very similar and highly correlated. The correlations between the measured and assumed angles of right ascension, declination, and rotation and their rates are 1.0 for zero time lag in all cases.

As in flight conditions, the differences between measured and generic attitudes are rate-dependent. The angular rates of the camera reach almost 2000 arcsec/s but are typically near 200 arcsec/s. The rates correspond to the low orbit height of the satellite. First-order polynomial fitting yields the dependency of the angular differences on the angular rates (Table 2).

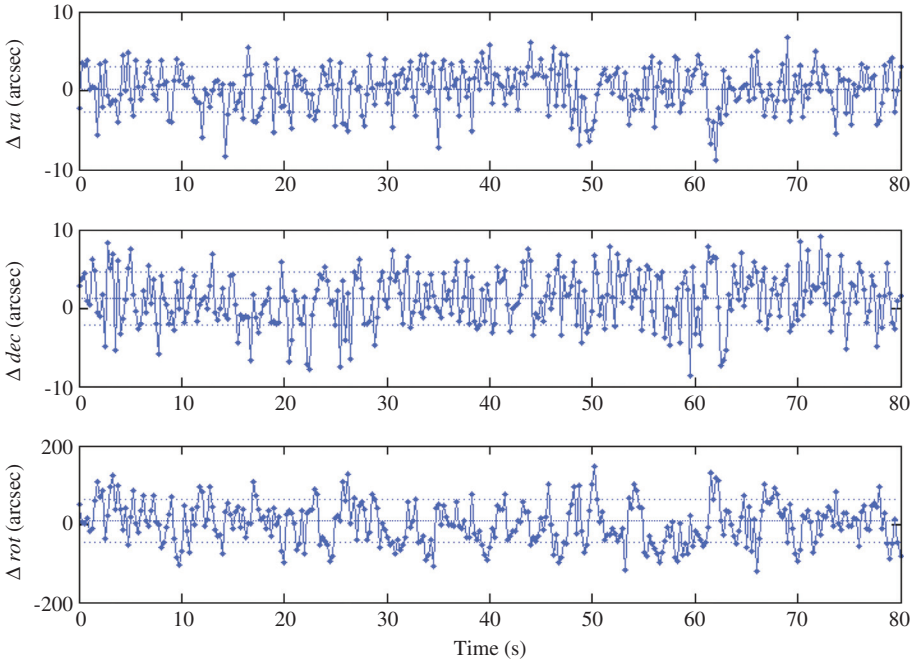


**Figure 5** Angular differences between camera attitude solutions and values assumed for image generation. Camera attitudes are calculated by viewing a static starry-sky image. Straight lines: mean difference, dashed line: one standard deviation interval around the mean (compare Table 1).

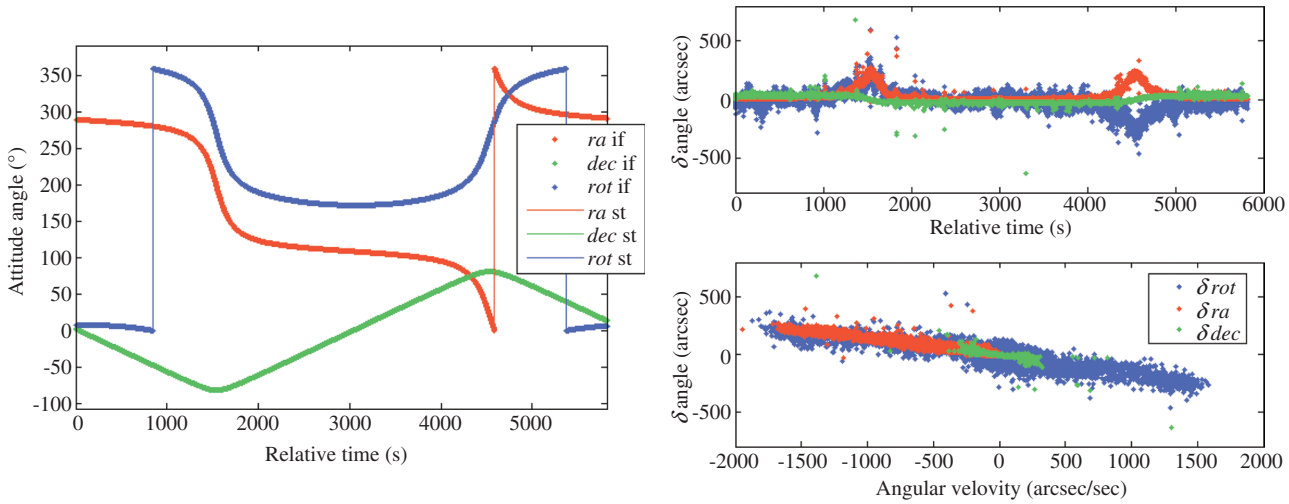


**Figure 6** Dynamic scene: (left) Attitudes assumed for the generation of star images (dots) and the solutions of the camera viewing the monitor (thin line). Assumed attitudes are based on the in-flight camera solutions of PRISMA. Jumps in attitude solutions are related to the 360° angular periodicity. The simulated attitudes represent camera solutions of the PRISMA satellite [4] during one true orbit. Note that the dots are so close that they appear as a thick line on top of the thin line. (right) Angular differences ($\delta$) for *ra*, *dec*, *rot* between camera solutions and values assumed for scene generation as function of flight time (top right) and angular velocity (lower right). Compare Table 2. Outliers correspond to missing or invalid solutions of the in-flight camera.

**Table 2** Linear dependency of the angular differences $\Delta$ on the angular rates for *ra*, right ascension, *dec*, declination, *rot*, rotation.

| | $\Delta/(d\Delta/dt)$ [″/(″/s)] | Offset [″/(″/s)] |
|---|---|---|
| $\Delta$(*ra*) (right ascension) | -0.1 | 1.4 |
| $\Delta$(*dec*) (declination) | -0.1 | 0.8 |
| $\Delta$(*rot*) (rotation) | -0.1 | -13.3 |

The offset values in rates in Table 2 represent the average differences a rate of zero arcsec/s (i.e., corresponding to still images) for the particular angle. The values confirm the observations from static star images.

The perfect correlation and the similarity between measured and assumed angles demonstrate that the stimulator is also able to represent dynamic scenes

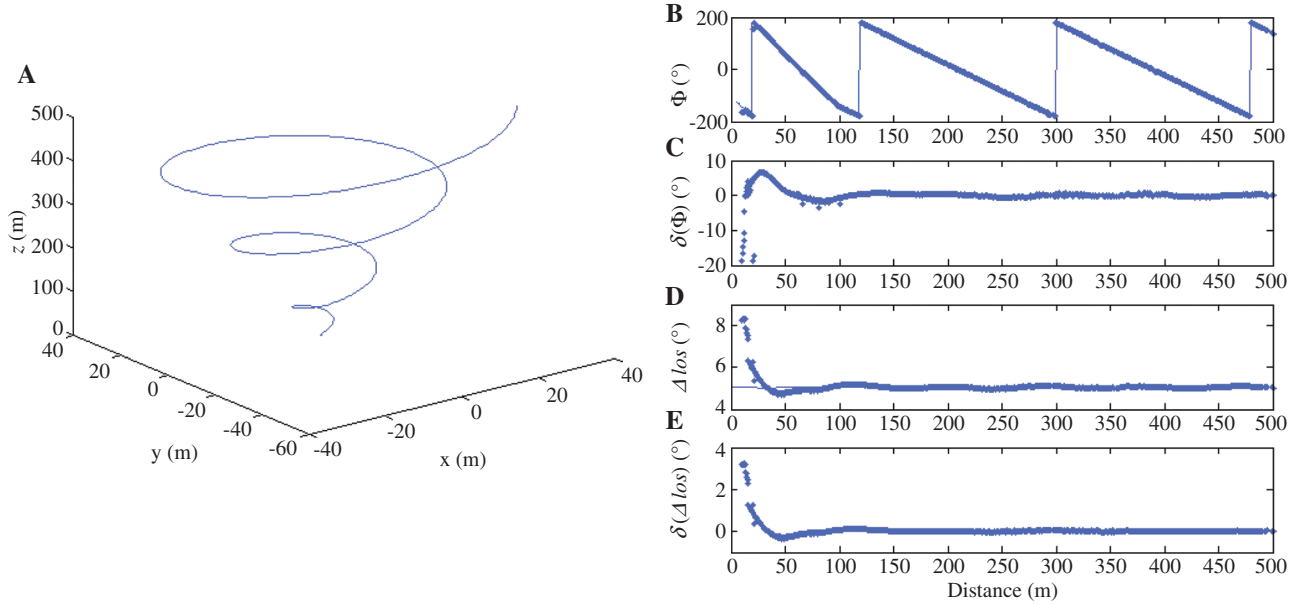


**Figure 7** (A) Simulated flight trajectory of the viewing camera in the reference frame of the viewing camera. Angle $\Phi$ is the azimuth in the CCD plane of the camera, $\Delta los$ is the angle to the boresight. Both angles refer to the center of gravity of the spacecraft. (B, D) Camera observations (dots) and assumed values (line) for $\Phi$ and $\Delta los$ and their differences $\delta(\Phi)$, $\delta(\Delta los)$ (dots in C, E).

with high fidelity and that the timing of system is appropriate.

### 4.3 Spacecraft rendezvous

The approach of a spacecraft toward another spacecraft's camera view is simulated along a weakly elliptical helical trajectory at distances between 500 m and close up (Figure 7, left). The viewed spacecraft is a small model representing the PRISMA Tango spacecraft. With a size of about 0.8×0.8×0.4 m (scaling: of 1:1) and complex surface features, it represents a simplification of the real satellite. Owing to the shape of the flight trajectory, the spacecraft is viewed by the camera at different angles and different sides. Spacecraft detection by the camera is automatic.

The viewed spacecraft is detected, and the line-of-sight in the field-of-view of the camera is computed fully autonomously by the camera and retrieved by telemetry/telecommands. Viewing the monitor of the stimulator, the spacecraft is detected and located (Figure 7, right). The line-of-sight angles $\Phi$ (azimuth) and $\Delta los$ (angle to camera boresight) are successfully retrieved. Owing to the extent of the spacecraft and the complexity of the surface properties, the illumination intensity of the spacecraft is not centered around the center of gravity of the spacecraft. Therefore, distance-dependent deviations in the line-of-sight solutions from assumed values are expected and observed. These deviations are most visible at distances <100 m (Figure 7, right).

## 5 Conclusion

An optical stimulator for vision-based system (OSVBS) has been successfully developed and tested. The stimulator enables the involvement of a navigation camera in the loop during the simulation of various critical spaceflight scenarios such as attitude determination from star observations and the rendezvous and docking of spacecraft.

The representativeness of the camera stimulation increases with the fidelity of the scene image generation and projection. It further depends on the ability of the system to create images with the correct geometry in the field-of-view. We have employed powerful computer programs for scene rendering and developed software tools that guarantee high accuracy of the image geometry. Currently, available monitors that meet the system criteria use LED technology and retain a certain level of background illumination and provide a limited dynamic range. For low-intensity condition such as starry-sky or extreme high-light conditions, e.g., with the Sun near, within the field-of-view, this may require an adjustment of the camera shutter or integration time. With the availability of OLED monitors, this issue is expected to diminish soon at least for low-light conditions. The modularity of the OSVBS supports this development.

Owing to the involvement of the camera, including the camera head unit, in the image processing chain, OSVBS reaches a higher level of realism than other simulators without a camera in the loop such as pure computer simulation or direct scene injection into the data processing unit of the camera. The high geometrical accuracy of the camera stimulation allows for flight-representative operation of the camera in the loop.

The system is composed of low-cost hardware components that can be easily replaced to adapt to changing requirements. The robustness and relative simplicity in the hardware design is accomplished by software-assisted optical calibration and image manipulation. The careful mechanical setup and the combination of optical calibration and image postprocessing result in camera stimulation with high image accuracy and with long-term stability.

OSVBS can be used during the development and testing of new optical navigation sensors, for design tests of spacecraft maneuvers and for the validation of Attitude Determination and Control Systems (ADCS) in open and closed loop modes.

**Acknowledgments:** The development of this stimulator has received funding from GMV Aerospace and Defense SA within the framework of a project of the European Space Agency (ESA). Two anonymous reviewers are acknowledged for their helpful comments and Kevin Flemming for editorial suggestions. Both have led to significant improvements of the manuscript. We thank the entire staff at DTU Space, Measurement and Instrumentation, for their enthusiastic support throughout the project.

Received July 30, 2013; accepted March 6, 2014

## References

[1] J.L. Jørgensen, A. Eiserman, C. Liebe and G. Jensen, in Proceedings of the 3rd ESA Symposium on Spacecraft Guidance, Navigation and Control Systems, ESTEC, ESA (1997).
[2] P.S. Jørgensen, J.L. Jørgensen, T. Denver and P. van den Breambussche, in Small Satellites for Earth Observation: Selected Proceedings of the 5th International Symposium of the IAA. Walter de Gruyter, 299-303, ISBN: 3-11-018851-1 (2005).
[3] M.M. Birnbaum, Acta Astron. 39, 763–773 (1996).
[4] J.L. Jørgensen and M. Benn, NordicSpace, 16–19 (2010).
[5] G. Rufino, D. Accardo, M. Grassi, G. Fasano, A. Renga and U. Tancredi, Int. J. Aerospace Eng. 2013, 13 pp. (2013).
[6] Astrium, A Minitiarized Star Tracker Optical Simulator. URL: http://www.astrium.eads.net/media/document/stos_2013-01.pdf, last visited: 15/10/2013 (2013).
[7] V. Barrena, P. Colmenarejo, D. Roessler, D.A.K. Pedersen and F. Ankersen, Use of In-Flight Data to Validate Mars Sample Return Autonomous RvD GNC, 63rd International Astronautical Congress, Naples, Paper code: IAC-12,D1,6,3,x16030 (2013).
[8] S. Parkes, I. Martin, M. Dunstan, D. Matthews and A. Milne, in 3rd International Workshop on Astrodynamics Tools and Techniques, ESTEC, ESA (2006).
[9] Celestia, http://www.shatters.net/celestia/, last visited on 15/10/2013.
[10] G. Bradski, A. Kaehler, in 'Learning OpenCV', (O'Reilly Media, Inc., Sebastopol, 2008). ISBN: 978-0-596-51613-0.
[11] D.C. Brown, Photogramm. Eng. 37, 855–866 (1971).
[12] J.G. Fryer and D.C. Brown, Photogramm. Eng. Remote Sens. 52, 51–58 (1986).

Dirk Roessler is responsible for the development of the hardware and the software of the stimulator. He worked at the Measurements and Instrumentation group at the National Space Institute, Technical University of Denmark, from 2011 to 2013. Roessler holds a diploma degree in Geophysics from the University of Leipzig, Germany and a doctoral degree in Geophysics from the University of Potsdam, Germany.

David A.K. Pedersen works with image analysis and develops methods and software related to DTU's microAdvanced Stellar Compass and Vision-Based System. Pedersen joined the Measurement and Instrumentation group at the National Space Institute, Technical University of Denmark 2011. Pedersen holds a MSc E.E. from the Technical University of Denmark.

Mathias Benn develops methods, software, and hardware related to DTU's microAdvanced Stellar compass and vision-based systems for closed-loop formation flying of spacecraft. He joined the Measurements and Instrumentation group at the National Space Institute, Technical University of Denmark, in 2007. Benn holds a MSc E.E. with focus on Space Technology and a PhD in Space Technology from the Technical University of Denmark.

John L. Jørgensen is Professor and Head of Measurement and Instrumentation division at the National Space Institute, Technical University of Denmark. Jørgensen is expert in space technology and systems such as rockets, satellites, and advanced measurement systems. He has developed the world's first fully autonomous star tracker camera. His research focus is on the development of technology for future spacecraft formation flying as a condition for many ambitious space missions such as manned expeditions to Mars, extremely large and precise telescopes, and Earth observation missions.